Using artificial neural networks and sliding mode control, the performance of hybrid renewable energy sources connected to the grid is improved

1)MOHAMMED YASEEN,2) TELLA DEEPA, 3)ALAGALA KEVIN,4)DONKA ANAND, 5)YAMALI SRINIVASU, 6) CH.VISHNU CHAKRAVARTHI

1.Student, Electrical and Electrical Engineering , Sanketika vidhya parishad engineering college, Visakhapatnam, Andhra Pradesh

2.Student, Electrical and Electrical Engineering, Sanketika vidhya parishad engineering college, Visakhapatnam, Andhra Pradesh

3.Student, Electrical and Electrical Engineering, Sanketika vidhya parishad engineering college, Visakhapatnam, Andhra Pradesh

4.Student, Electrical and Electrical Engineering, Sanketika vidhya parishad engineering college, Visakhapatnam, Andhra Pradesh

5.Student, Electrical and Electrical Engineering, Sanketika vidhya parishad engineering college, Visakhapatnam, Andhra Pradesh

6 Assistant Professor , Electrical and Electrical Engineering , Sanketika vidhya parishad engineering college, Visakhapatnam, Andhra Pradesh

ABSTRACT

In hybrid renewable energy source (HRES) systems, the primary goal of this research is to evaluate and analyse three different types of controllers for three-phase DC-AC inverters. To do this, two contemporary controllers based on artificial neural network and sliding mode control (SMC) methodologies are designed and compared. Among the HRESs are solar (PV), step-up transformers connecting transmission lines, battery storage systems and wind turbines to infinite bus bars. Both voltage control and current regulation are used by the developed controllers at the inverter side. To provide a voltage demand at the point of common coupling, a DC–DC boost converter is used (PCC). Next, a presentation of the HRES formulation using the created controllers follows. It is thought that the created controllers will function under a range of solar radiation, temperature, and wind speed loading scenarios. To confirm the effectiveness of the constructed controllers, MATLAB/Simulink is used to simulate the HRESs with the controllers. The acquired outcomes show that adaptive SMC additionally. When compared to traditional PI control, artificial neural network (ANN) control techniques yield superior outcomes in terms of input power, output power, current, and voltage.

Keywords: *sliding mode control, hybrid renewable energy system Artificial Neural Network*

1. Introduction

Most people on the planet favour switching from diesel to renewable energy. Because it produces no pollution, renewable energy is also known as clean energy. The globe requires safe and environmentally friendly energy sources, as the pollution from fossil fuel-based energy has been making the world air quality index worse every day [1].

Industry research is heavily reliant on the use of controllers. This facilitates obtaining the necessary responses from the various kinds of controllers that are employed in research. Three different kinds of inverter controllers are being studied in this study generally used. In industries where an automatic controller is required to regulate a process, PI control is a common kind of traditional control [2, 3]. Adaptive control, often known as sliding mode control (SMC), is a kind of discontinuous control. It is a reliable control mechanism [4]. SMC preserves trajectories on the sliding surface and variable structure and is made up of similar control [5]. SMC was utilised to create appropriate parameters for the conventional SMC, which improved convergence performance [6]. Conventional because of its quick response time, robustness against uncertainties and disturbances, and ease of implementation, SMC has been used extensively in nonlinear systems [7]. ANN is a sophisticated control method.

Because of their great capacity for pattern recognition, artificial neural networks (ANNs) have found application in a wide range of engineering fields as an estimating method [8]. One advantage of ANNs is that they do not require any understanding of internal system parameters, which reduces computational effort and yields a more compact solution [9]. Furthermore, extremely difficult issues have been resolved by ANNs [10].

An ANN with PI control was created by Kalam et al. in [11] for the direct power control of a grid-connected PV system. Yoo et al. showed effective control in [12] with a microgrid utilising the PQ Strategy. Fuzzy logic control was presented by the authors of [13] for a grid-connected PV. Ayvaz et al. created ANN applications for a balanced, long-term early warning system in [14]. In [15], a neural network with a temporal delay was presented in an illustration application. A PV with SMC at three phase grids linked with an LCL filter was created by the authors of [16]. Zhang et al. transformed the economic dispatch problem into a prediction problem in [17] to provide a model predictive control for HRES stability problems. Examining the publications indicates that most of the literature's works focused on a single control issue in HRESs using an inverter-side controller without any meaningful comparison talks.

SMC was exclusively employed by the authors of [18] for a microgrid's hybrid sources. Chen and colleagues presented hybrid AC/DC microgrids in [19] that were able to simulate synchronous generators qualities. Without the use of a control strategy, the authors of [20] created a hybrid photovoltaic system using a fuel cell source. For a wind turbine, Mili et al. employed a fuzzy-based adaptive SMC in [21]. A hybrid wind/battery power system using model predictive control for voltage–power and current–power was presented by Shan et al. in [22]. Examining the manuscripts demonstrates that there are little HRES comparisons between PI, SMC, and ANN controllers-based inverters connected to the grid. This adds even more incentive to create sophisticated and adaptable controllers for HRES systems.

Although there is a wealth of literature on SMC and ANN in many fields, studies comparing ANN and SM controllers for grid-connected HRES are not common. The following are the contributions this study provides to the literature for such a difficult undertaking. (1) Creating ANN and SMC control methods. (2) Evaluating the developed SMC and ANN's effectiveness considering the variable conditions of PVs (temperature and irradiance) and wind turbines (wind speed) by conducting a fair comparison with classical PI controllers, integral order PI controllers, adaptive controllers, and advanced controllers. (3) Creating a dynamic MATLAB/Simulink formulation and presenting a mathematical formulation for an HRES system using the controllers that were designed.

This paper's HRES combines wind turbine and photovoltaic systems with battery storage. Renewable resources are those that occur naturally and can be converted into energy renewable energy sources that replenish on a human timeline, including wind and sunshine, and an energy storage system is employed to meet the demand for power during inclement weather [23]. The wind turbine is a permanent magnet synchronous generator (PMSG), the PV array is a sun-power SPR-305E-WHT-D, and the battery storage is a Ni-MH battery, 200 V, 6.5 Ah. DC-DC converters are used to connect these three categories of resources.

A DC-DC boost converter has been used to regulate DC voltages from various resources and to elevate the voltage from the sources to the DC-bus bar [24]. The PV origin uses increasing conductance to reach MPPT. Additionally, MPPT is used in the wind generation system using PI controllers. A PLL is used to convert DC power from the DC-bus bar to a three-phase inverter. A positive and negative line can be converted to three-phase AC electricity using the PLL [25].

This is how the rest of the paper is structured. Section 2 provides a description of the system. Section 3 introduces the suggested controllers. Results and discussions of the simulation are provided in Sect. 4. Finally, Sect. 5 provides some conclusions.

This study proposes a method for analysing and implementing HRESs to three-phase microgrids using three different inverter control strategies. These three control strategies are ANN, SMC, and PI. The findings indicate that the adaptive SMC control. When compared to the traditional PI control, and sophisticated ANN control produce good results at the input and output powers, currents, and voltages.

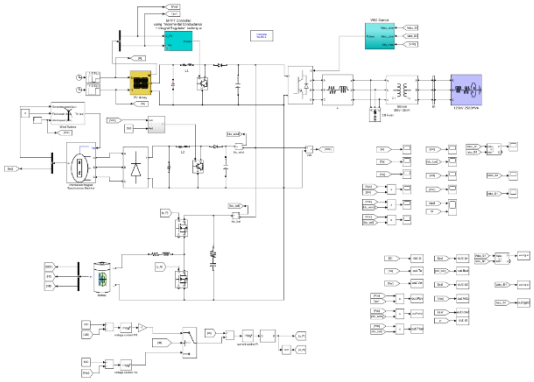

Fig. 1 Configuration of a hybrid renewable energy generation system

2. System description

The HRES suggested in this paper is seen in Figure 1. The system is made up of a step-up transformer, a DC-DC converter, a DC link, a three-phase inverter, PI, SMC, and ANN controllers, a wind energy system, a PV energy system, and a battery storage system. The grid and the three-phase transformer.

2.1 PV system

An essential stage in the analysis and design of photovoltaic control systems is the PV mathematical modelling of PV panels. A PV cell's single diode model is shown in Figure 2. This PV cell's electrical equivalent circuit presents the serial resistance's effect Rs without considering the impact of shunt resistance Rsh.

The following equations [23] illustrate the link between the PV cell's voltage and current:

$$I_c = I_{ph} - I_o\left\{e^{\left[\frac{q}{aKT}(V_c + I_c R_s)\right]} - 1\right\} \quad (1)$$

$$V_c = \frac{aKT}{q}\ln\left(\frac{I_{ph} + I_o - I_c}{I_o}\right) - I_c R_s \quad (2)$$

$$I = I_{ph} - I_o\left\{e^{\left[\frac{q}{n_s aKT}(V + n_s I R_s)\right]} - 1\right\} \quad (3)$$

$$V = \frac{n_s aKT}{q}\ln\left(\frac{I_{ph} + I_o - I}{I_o}\right) - n_s I R_s \quad (4)$$

where:

$$I_{ph} = \frac{G}{1000}\left[I_{sc} + K_{th}(T - T_r)\right] \quad (5)$$

$$I_o = I_{or}\left(\frac{T}{T_r}\right)^3 e^{\left[\frac{qE_g}{aK}\left(\frac{1}{T_r} - \frac{1}{T}\right)\right]} \quad (6)$$

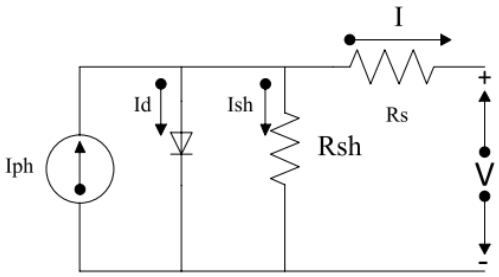

Fig. 2 PV cell equivalent circuit [2]

The PV cell's output current (Ic) is calculated from Fig. 2 by subtracting the photo-generated current (Iph) and the diode current (Id), as shown in Eq. (1). Consequently, the output voltage of the PV cell is determined using Equation (2). For a PV module with ns cells, the voltage (V), output current (I), and series-connected cells are shown in (3) and (4), respectively. Equation (5) provides the photo-generation as a function of temperature (T) and solar radiation (G), whereas Equation (6) provides an estimate of the reverse saturation current (Io).

The PV module's output voltage multiplied by its output current yields the module output power, which can be found using Eq. (7) [26].

$$P = VI \tag{7}$$

Fig. 3 displays the I-V and P-V curves derived from the PV model. The PV module's global MPPT is found by applying the integrated regulator technique in conjunction with incremental conductance.

2.2 Wind turbine

A popular form of wind turbine energy source is the permanent magnetic synchronous generator (PMSG). Because it has a magnetic field rather than a winding, it has more gravity in wind-energy applications. In Furthermore, it offers several benefits. Its speed is overly fast.

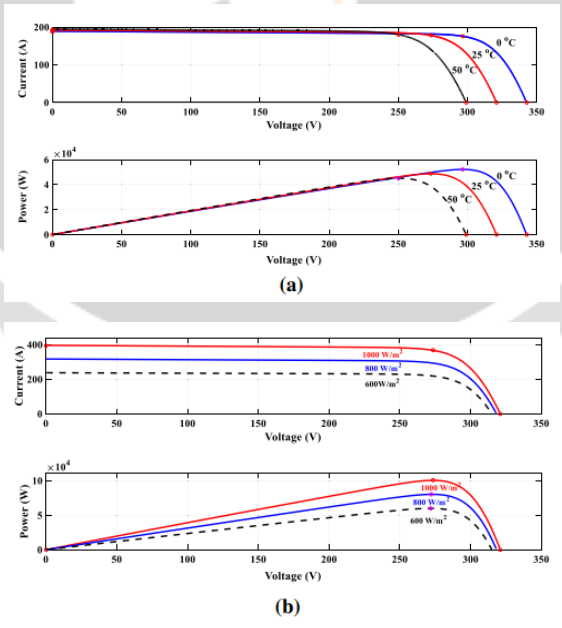

Fig. 3 PV output characteristics I–V and P–V curves at: a different temperature; b different irradiations

generation, including enhanced energy capture, MPP operation, enhanced efficiency, and high-quality power [27]. In wind energy applications, the PMSG has drawn a lot of attention due to its high efficiency, and operates with a high-power factor [28].

$$E = \frac{1}{2} m * v^2 \quad (8)$$

$$p = \frac{dE}{dt} = \frac{1}{2} \dot{m} * v^2 \quad (9)$$

where:

$$\dot{m} = \rho A v \quad (10)$$

$$p = 0.5 \rho A v^3 \quad (11)$$

Equation (12) calculates the wind turbines' real mechanical capacity to produce wind energy. Furthermore, the mechanical torque can be found in (13).

$$P_m = \frac{1}{2} \rho \pi R^2 C_p V_w^3 = K_2 C_p V_w^3 \quad (12)$$

$$T_m = \frac{P_m}{w_m} \quad (13)$$

The machine's mathematical model voltages are computed in (14).

$$V_{dq0} = K_{CP} V_{abc} \quad (14)$$

A wind turbine's tip speed ratio can be computed using equation (15). A typical Cp against λr curve is displayed in Figure 4a for the wind turbine's PMSG. To track a wind turbine's maximum power, it must run at its ideal tip speed ratio (λopt), which yields the corresponding maximum power coefficient (Cpmax), which can be found in Fig. 4b. Thus, from Fig. 4d, the maximum power is obtained. The control circuit shown in Fig. 4c is used to regulate this.

$$\lambda_r = \frac{w_m R}{V_w} \text{ where } w_m = K_1 N \quad (15)$$

The blade pitch angle (β) is limited by a controller based on the generator speed. As shown, the wind turbine model uses the pitch angle, generator speed, and wind speed to offer the PMSG generator the necessary mechanical thrust in Figure 4c. The generator and wind speeds are used to control the ideal tip speed ratio (λopt). To maximise the energy recovered from the wind, another controller is used to calculate the ideal power coefficient (CP), as seen in

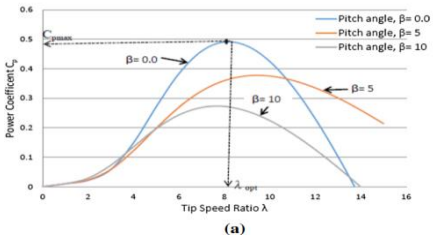

(a)

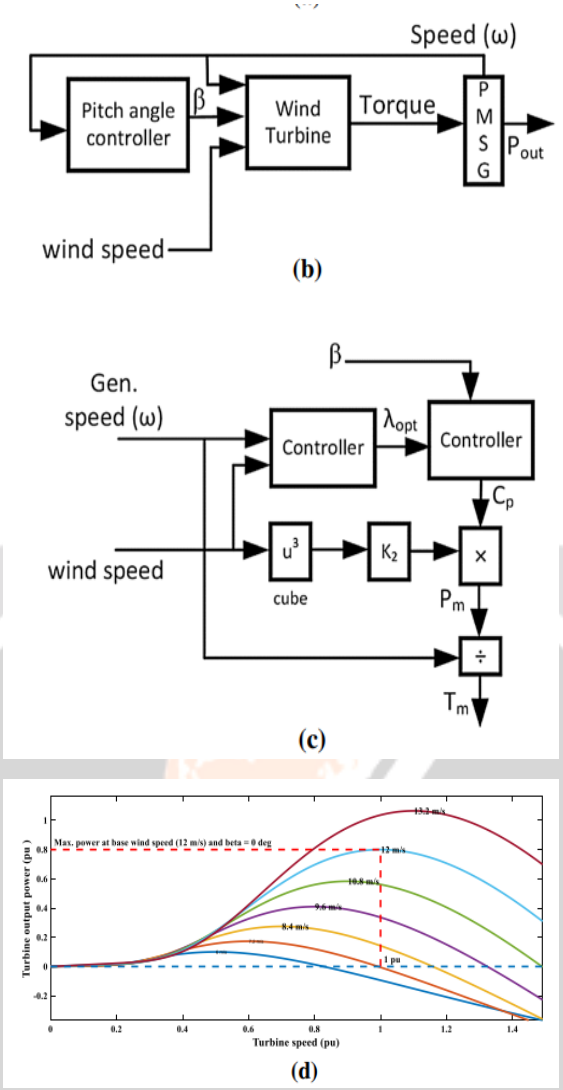

Fig. 4 Wind turbine control circuit: a typical Cp versus λr curve; b wind turbine controller; c wind turbine model; d turbine speed versus output power (pu)

Based on the pitch angle (β) and the ideal tip speed ratio (Fopt), Figure 4a was created. The DC/DC boost converter's topology, which is given in Sect. 2.4, was applied to the wind turbine-based PMSG as well as the PV module. A three-phase bridge rectifier is used to rectify the power that the PMSG collects before being sent into the DC/DC converter. The DC/AC converter at this bus receives the energy gathered from all the resources and works to optimise the amount of electricity sent to the grid.

2.3 Battery storage

This HRES uses a Ni-MH battery that is coupled to a DC-DC boost converter. Because renewable energy sources are intermittent, it is crucial to this system [29]. The power source storage is used extensively, for example, to provide local loads and the grid's power demands.

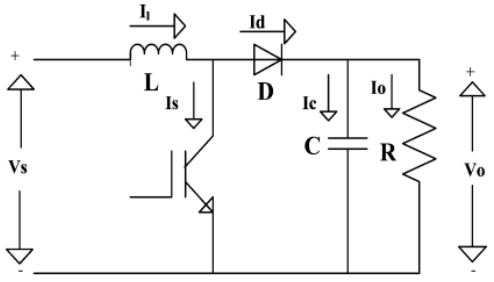

Fig. 5 DC–DC boost converter [30]

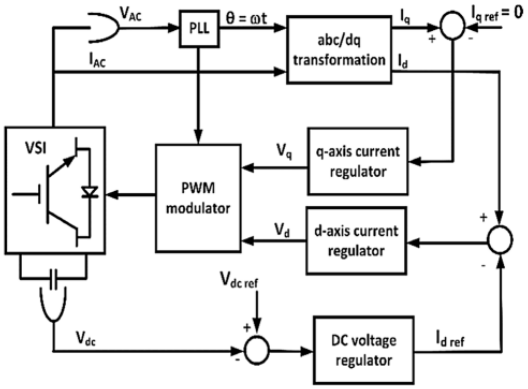

Fig. 6 Block of the controller for the inverter of a system

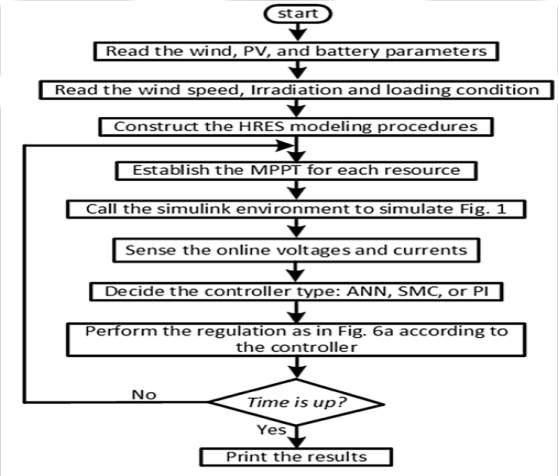

Fig. 7 Flow chart of the proposed control techniques

2.4 DC–DC converter

The DC voltage level is adjusted using the DC–DC converter [2]. From Eq. 16, the output voltage is found. In Fig. 5, the boost converter is displayed.

$$Vo = \frac{Vs}{1 - D} \quad (16)$$

3. Proposed controllers

The total controller system employs four phases at once, as Fig. 6 illustrates. The controller first uses Park's formula to translate the stationary reference frame voltages and currents into the matching revolving reference frame values changes. As a result, the commanded references are compared to the currents (Iq and Id). The reference current (Iqref), which is subsequently adjusted to zero to maximise the power supplied to the grid, is controlled by a process that governs the AC voltage in the second control loop. This process controls the magnitude of the AC voltage from the VSI. As a result, the VSI is running at unity power factor. The regulator receives the voltage from the DC-link capacitor and uses it to set the d-axis current command (Idref). The purpose of the second and third controls is specifically to adjust the VSI output currents' phase and size at suitable values for the wind and solar radiation under various operating situations in order to preserve the inverter's output power factor [31]. The PWM block receives the outputs from the current regulators and transfers them to the VSI electronic switches. The AC/DC VSI that is utilised to integrate the HRES system raises another significant concern. Consequently, frequency sensing employs the PLL loop to generate the angle (θ), which in turn controls the operation of the other regulators and electrical switches harmony to feed energy into the primary grid. A comprehensive flowchart of the suggested control techniques is shown in Figure 7, where each regulator is

selected based on the type of controller. The online operation of the PLL and voltage and current sensing in all controller types maintains the DC/AC VSI in sync with the primary grid frequency.

3.1 Classic proportional integral controller (PI)

The most often used kind of industrial control is still PI control. One kind of traditional control is the PI controller. Two constant parameters are used in PI control: Kp for the proportional term and for the integral term, use Ki [32]. The PI controller is regarded as an automated controller and is a significant approach that has been applied to HRESs [33]. The stable state error for step input under the long-term conditions is zero. Through a control element, like in (17), the total of the two terms modifies the process. A schematic diagram of the PI block's internal organisation is displayed in Figure 8.

$$G(s) = K_p + \frac{K_i}{s} \quad (17)$$

3.2 Sliding mode control (SMC)

Variable structure system controllers employ a sort of discontinuous control called SMC. This approach necessitates measurements and involves intricate calculations [34]. This Harding et al. created the control approach [35]. SMC is accessible for HRES regulation.

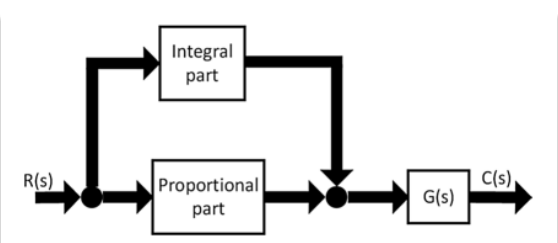

Fig. 8 Internal structure of a PI block

The operational point in SMC control systems travels through or inside the sliding surface. The controller output is made up of two words at any given time. The first one shows the error's area versus time, while the second shows how big the error is. Using sliding mode control, the percentage gain can improve the output controller's response and the system's control accuracy. The general equations providing a straightforward explanation of SMC for the HRES system input are provided in (18) and (19).

$$\dot{X} = f(x,t) + g(x,t)u \quad (18)$$

$$y = x(h,t) \quad (19)$$

This is how the sliding surface design is produced. The definition of a specific scalar function of the system state, σ (x): Rn→ R, is given first. The sliding surface frequently depends on a specific number of its derivatives as well as the tracking error ey(t).

$$\sigma = \sigma(e, \dot{e}, \ldots e^{(k)}) \quad (20)$$

The function σ ought to be chosen in a manner that results in a stable differential equation upon its disappearance at the steady-state. The differential equations ey(t) solution will gradually tend to zero. A linear combination of the following, as in (21) is the most common selection for the sliding manifold (surface).

$$\sigma = e^{(k)} + \sum_{i=1}^{k-i} c_i e^{(i)} \quad (21)$$

A first-order combination in the system under investigation is examined using Eq. (22).

$$\sigma = \dot{e} + ec_o$$

This is how the control input design is obtained. Choosing a controller action at the sliding manifold (surface) is the primary goal of this stage. The ability of the control action is too direct σ to zero within a specified time frame. In this study, the HRES inverter is controlled using the usual (or first-order) sliding mode control. All throughout the manifold, there is constant control. Fig. 9 depicts an SMC block of a VS regulator controller. Fig. 10 depicts a current regulator controller block of an SMC.

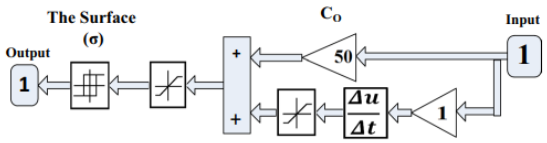

Fig. 9 SMC module of a voltage regulator controller

$$\sigma = 0, u = -Usgn(\sigma) \quad (23)$$

$$u = \begin{cases} -U\sigma > 0 \\ U\sigma > 0 \end{cases} \quad (24)]$$

3.3 Artificial neural network (ANN)

One kind of intelligent control, or advanced control, is artificial neural network (ANN). This kind of controller is employed to address challenging issues. HRESs can be managed using ANN. An input layer, an output layer, and several hidden layers make up ANN control. The input layer relies on control of the current for a voltage regulator controller, it is dependent upon voltage, and in the case of a current regulator controller, it is dependent upon voltage [36].

There are several neurons in each layer of the ANN structure. Every neuron in a layer is linked to every other neuron in the layer below. An ANN in the HRES uses twelve hidden levels. Three regulators are used by the overall controller in Figure 6. The first one sets the d-axis current command by using the DC link capacitor voltage error. As a result, there is just one output and one input signal.

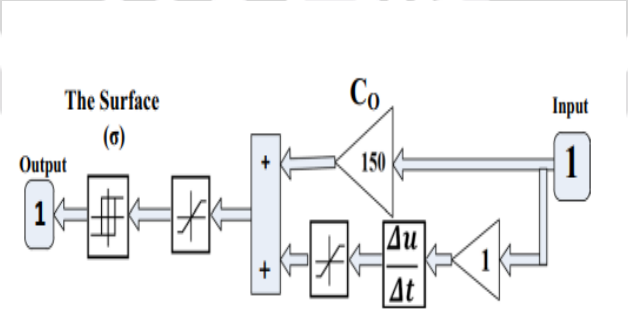

Fig. 10 SMC module of a current regulator controller

Table 1 Neural network characteristics

Number of inputs		1
Number of outputs		1
Number of layers		2
Number of hidden layers		12
Number of weightings		31
Matlab used function		Feedforwardnet
Training method		Levenberg–Marquardt backpropagation
d-axis regulator	RMSE	0.009
	RE	0.85
	R_{cor}	0.828
q-axis regulator	RMSE	0.002
	RE	0.095
	R_{cor}	0.954
DC-regulator	RMSE	0.162
	RE	0.15
	R_{cor}	0.792

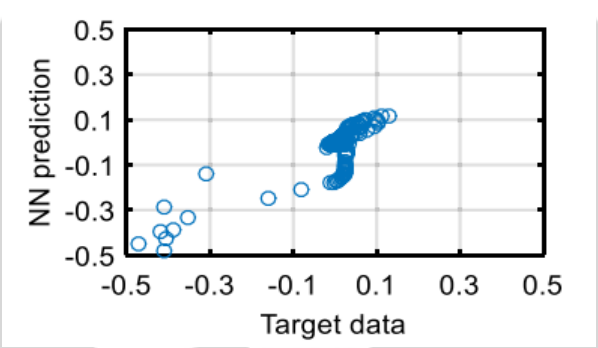

Fig. 11 Neural network training regression in a d-axis regulator

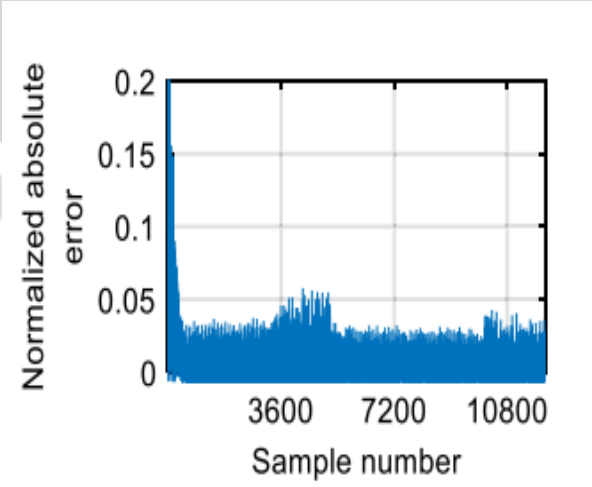

Fig. 12 Normalized absolute error of a d-axis regulator

The other regulators only use one error input signal as well. The output is therefore also a single output signal. The generated ANN was validated using the root-mean-square error (RMSE). The correlation coefficient (Rcor) and relative error (RE) provided in equations (25) to (27) are examined. The developed ANN's characteristics are listed in Table 1, where it showed acceptable correlation values.

$$\mathrm{RMSE} = \sqrt{\frac{1}{n_T}\sum_{n=1}^{n_T}(y_P - y_T)^2} \quad (25)$$

$$\mathrm{RE} = \frac{\mathrm{RMSE}}{\bar{y}_p} \quad (26)$$

$$R_{cor} = \frac{\sum_{i\epsilon T}(y_p - \bar{y}_p)\sum_{i\epsilon T}(y_T - \bar{y}_T)}{\sqrt{\sum_{i\epsilon T}(y_p - \bar{y}_p)}\sqrt{\sum_{i\epsilon T}(y_T - \bar{y}_T)}} \quad (27)$$

The developed neural networks of the three regulators are trained in this research using the inputs and outputs of the conventional PI controllers. Consequently, the targets are the PI regulators' output commands.

Table 2 Power system parameters

Parameter	Value
PV parameters	
PV maximum power of module	305.23 W
Parallel strings of PV array	66
Series-connected modules per string	5
Inductance of boost converter	5e-3 H
Resistance of boost converter	0.005 'Ω'
Capacitance of boost converter	100e-6 F
Wind parameters	
Mechanical of Wind output power	200,000 W
Base wind speed	12 m/s
Maximum power at base wind speed	0.8 pu
Base power of the electrical generator	200,000/0.9 VA
Pitch angle beta	0 deg
Resistance of rectifier	100 Ohms
Capacitance of rectifier	0.1e–6 F
P_{wind}	69.7KW
Battery parameters	
Nominal voltage of battery	300 V
Rated capacity	6.5 Ah
$P_{Battery}$	22KW
Grid parameters	
Step up transformer	260 V/25 kV
Grid voltage	20,000 V
Grid frequency	60 Hz

Table 3 Control system parameters

K_p current regulatory control at PI	0.3
K_i current regulatory control at PI	20
K_p Voltage source control at PI	7
K_i Voltage source control at PI	800
Reference voltage of DC link	500 V
Hidden layer at ANN	12
(C_o) in SMC at current regulatory control	150
(C_o) in SMC at voltage source control	50
The surface (σ): switching on point at current regulator control	0.5
The surface (σ): switching off point at current regulator control	− 0.47
The surface (σ): switching on point at current regulator control	0.9
The surface (σ): switching off point at current regulator control	− 0.47

equivalents. The ANN forecast is displayed against the intended data in Figure 11. At the d-axis regulator, the absolute normalised error is displayed in Fig. 12. The actions of the developed ANN are regarded as acceptable. This is

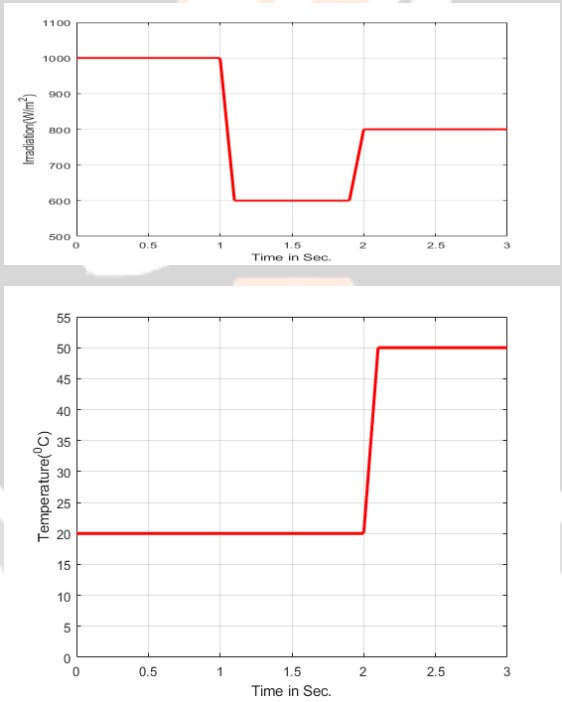

Fig. 13 Weather conditions: a changing irradiation of a PV; b changing temperature of a PV

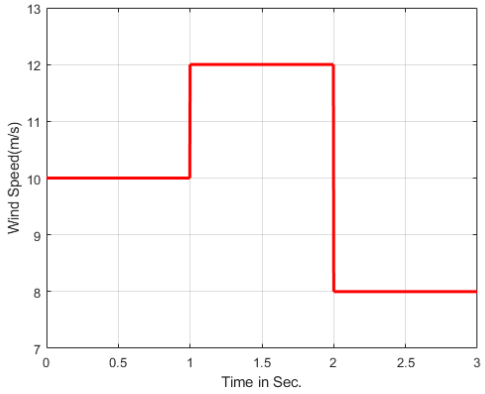

Fig. 14 Wind profile for a wind turbine

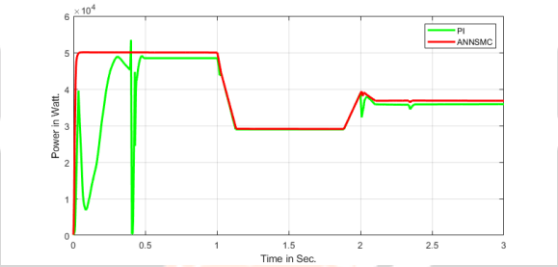

Fig. 15 PV output power

revealed by the straight-line approximation of the primary data components and the correlation values, which are close to 1. The purpose of employing an ANN is associated with because of this, ANNs are regarded as regression techniques. As a result, they could produce better outcomes than their PI colleagues.

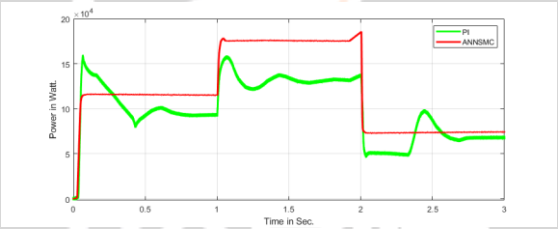

Fig. 16 Wind turbine output power

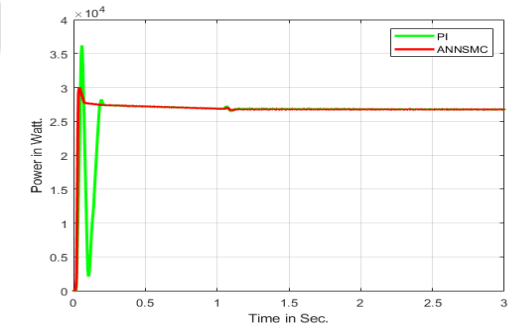

Fig. 17 Battery output power

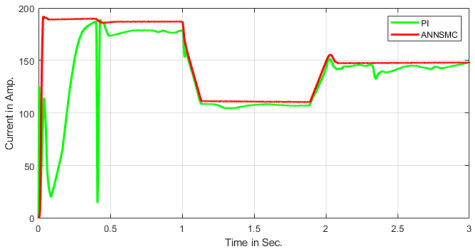

Fig. 18 PV current of controllers

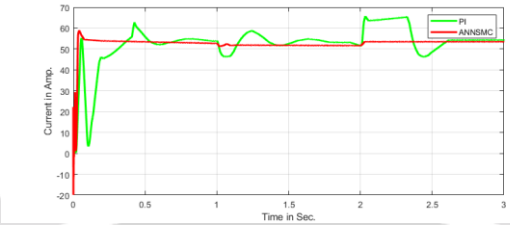

Fig. 19 Battery storage current of controllers

4. Simulation results and discussions

4.1 Results under ramp in solar radiation and step of wind speed

Tables 2 and 3 contain specifics on the system. To confirm the effectiveness of the controllers that were designed, Figs. 13 and 14 have their temperature, wind speed, and radiation levels altered. This affects the voltage, current, and output power. Operating variations of the PV module's temperature, irradiation, and wind speed are shown in Figures 13 and 14, respectively. Every parameter for the controller and simulation

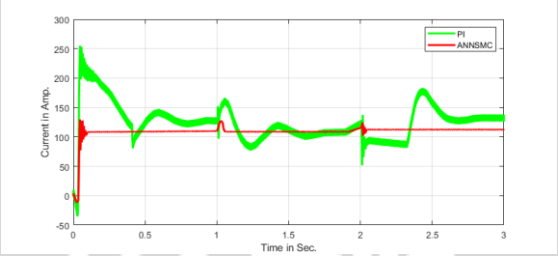

Fig. 20 Stator currents of a wind turbine at the d-axis currents for three controllers

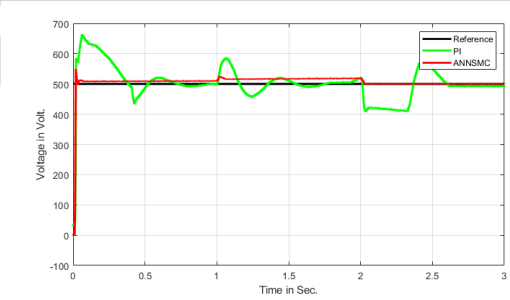

Fig. 21 Output boost converter of three controllers

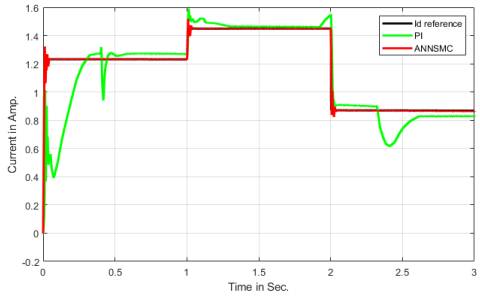

Fig. 22 Injected current control of three controllers

find themselves in the appendix. The MATLAB/Simulink environment is used to run the following simulations on the grid side and the resources side.

Considering the setup depicted in Fig. 1, the PV powers are displayed for the ANN, SMC, and PI controllers, respectively, in Fig. 15. Regarding the PV electricity delivered, the SMC and ANN consistently produce satisfactory results. But from 0 to 0.5 s, the PI controller performs the worst and exhibits the most ripples. The PMSG's output power is displayed in Figure 16. The robustness of the constructed SMC and ANN controllers was confirmed, and they produce good results. At first, the PI reports overshooting. After that, it gives overshooting at 2.5 s and undershooting at 0.5 s. The battery storage system's output power is shown in Figure 17. With a longer settling time, the PI controller. In contrast to the designed adaptive and advanced controllers, which demonstrated good performance with the minimum settling time, the damped overshoots and undershoots were observed.

Three different types of controllers' PV currents are displayed in Figure 18. From 0 to 0.5 s, the classic control performs poorly and produces waves. Nonetheless, ANN and SMC provide good performance and fulfilling outcomes about the PV current that is provided. The currents used by the batteries to store

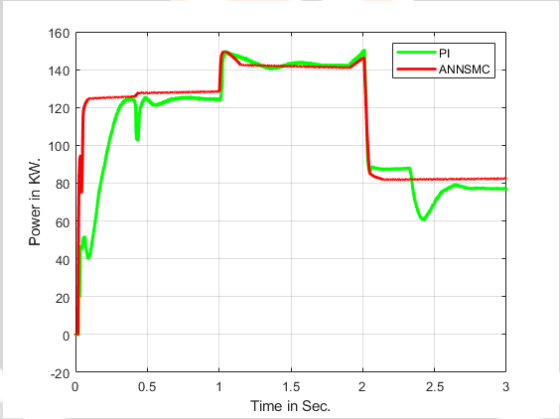

Fig. 23 Active grid power of three controllers

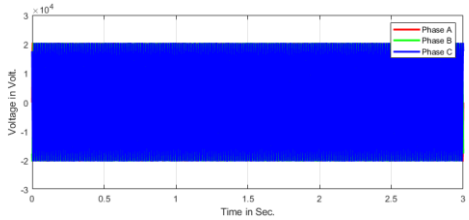

Fig. 24 Output grid voltages profile

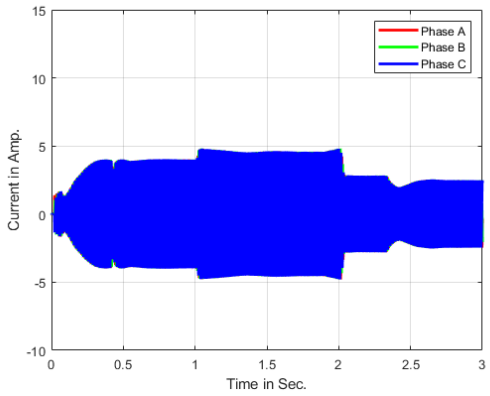

26 Grid current using SMC

Three different controller types are depicted in Fig. 19. There is an initial overshooting experienced by the ANN and SMC controllers. Still, they consistently produce positive outcomes. The PI control first experienced undershooting and displays the worst times were 0.5, 1, and 2.5 seconds.

A wind turbine's stator current for each of the three types of controllers is displayed at the d-axis currents in Figure 20. When compared to the traditional PI controller, the created SMC and ANN controllers exhibit satisfactory transitions with the least number of ripples under various weather disturbances. The PI controller displays an extended settling time along with inadequate

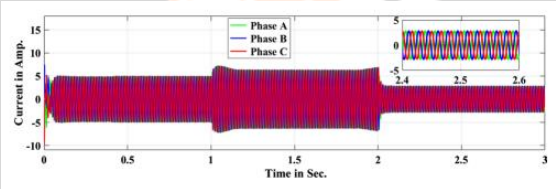

Fig. 27 Grid current using ANN

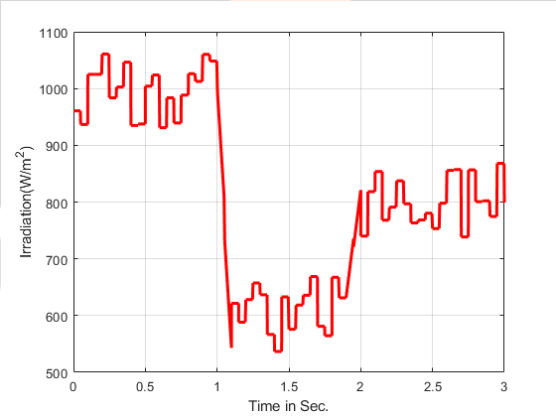

Fig. 28 Irradiance under a random changed profile

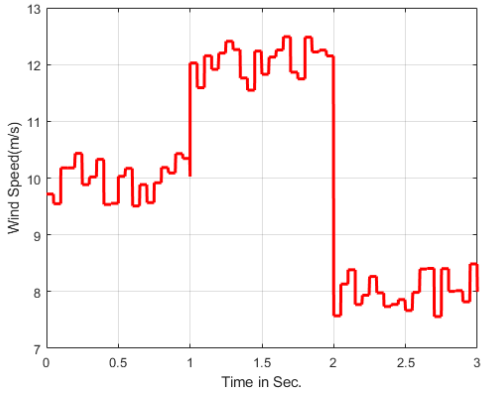

Fig. 29 Wind speed under a random changed profile

overshoots and lengthier settling times at 0.5, 1 and 2.5 seconds in addition to the start time. The output voltage for the DC–DC is displayed in Figure 21 three controllers' boost converter. Most of the time, the PI control produces results that are good enough to track the reference line. However, because of their reduced ripples to trace the reference line, the adaptive and sophisticated approaches produce the greatest results at 2-3 s. The three HRES controllers injected current control is displayed in Figure 22. PI control, as demonstrated in the zoomed-in picture of Fig. 22, does not follow the reference line at the start.

The created SMC and ANN approaches, on the other hand, track the current (Id) reference line consistently and produce good results. Power was injected by the grid is shown in Fig. 23 using the built PI, SMC, and ANN controllers. Under all variations in wind speed and sun radiation, the ANN and SMC respond satisfactorily. Nevertheless, because the PI controller performs poorly in response to variations in wind speed and radiation at the start (0–0.5 s) and 2.5 s, the results are not up to par.

Fig. 24 shows the inverter output voltage to the three-phase grid. Since the grid has rules, all three types of controllers provide the same output voltage (20 KV). Currents were injected by the grid via the created. Figs. 25, 26, and 27 display controllers. In comparison to the developed SMC and the classical PI control, the ANN control performs satisfactorily in terms of overshoots. When compared to the other controller, ANN, and SMC function satisfactorily, according to the findings in Figs. 26, 27. The inverter's functioning is swiftly and ripple-free thanks to the sophisticated and adaptable controls. On the other hand, in contrast to the other controllers, the PI control feeds the utility grid with less current.

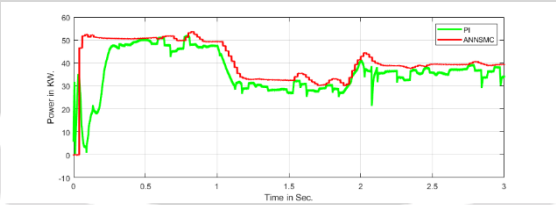

Fig. 30 Performance analysis of the PV power of three controllers

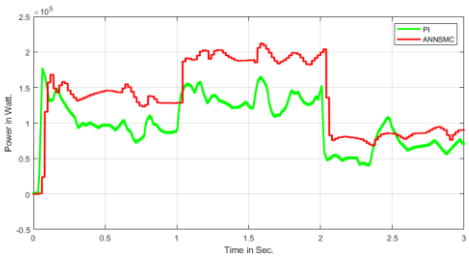

Fig. 31 Performance analysis of the active wind power of three controllers

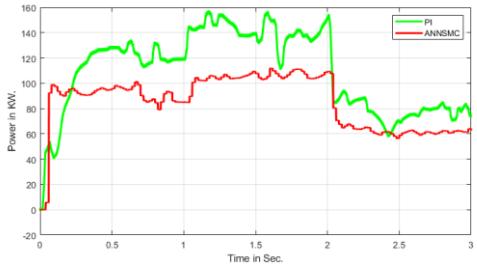

Fig. 32 Performance analysis of the active grid power of three controllers

Less power is sent to the grid because of this. When compared to the other, the PI control performs poorly two controllers—the ANN, SMC, and PI controllers at 2.4–2.6 s—as seen in the enlarged photographs. At 2.5 s, the PI does not produce good results. On the other hand, SMC, and ANN work exceptionally well at the output grid current.

4.2 Results under random changes in solar radiation and wind speed

Figures 28 and 29 show how solar radiation and wind speed fluctuate under random profiles, respectively. The PV output power performance comparison employing PI, SMC, and ANN controllers is displayed in Figure 30. Under erratic variations in wind and sun radiation. It is evident from a comparison of the PV system power using the three techniques that the controllers generated by SMC and ANN outperform PI in maintaining system stability and tracking the maximum PV power under arbitrary changes in parameters.

As illustrated in Fig. 31, the output wind power via PI, SMC, and ANN controller. Fig. 32 shows the effectiveness of the active power supplied to the main grid. However, the designed SMC and ANN controller showed a satisfactory reaction, and it was confirmed that they were robust under windy conditions that are unclear due to speed and solar radiation.

5. Conclusion

In this research, two contemporary controllers for three-phase grid-connected HRES were compared. To address the issue of transmitting power to the main grid, current and voltage regulators were developed. The evolved. When it comes to maintaining the stability of the HRES under varying wind speeds, irradiations, and loading circumstances, SMC and ANN are highly capable. A fair comparison with the traditional PI controller showed the effectiveness of the SMC and ANN controllers. The following conclusions can be made from the outcomes of the digital simulation. (1) With fast settling times, the developed controls are simple to use and very effective at damping out oscillations. Because the developed regulators rely on voltage at the DC-link in addition to voltages and currents at the inverter side without complex power measurements, they avoid complex signal measurements. Next, the HRES used in this study is seen as a first step towards improving the electricity supplied to the grid. It appears that the power delivered to the grid is more affected by variations in wind speed and solar radiation than by the ambient temperature of photovoltaic cells.

Therefore, for future work, this paper suggests using the created adaptive SMC with the advanced ANN controller. Among all the outcomes that were acquired, both the adaptive. When compared to the traditional (PI) control, the advanced control (ANN) and the supplementary motor control (SMC) provide satisfactory results at input power, output power, current, and voltages.

References

1. Lal, D.K., Dash, B.B., Akella, A.K.: Optimization of PV/wind/ micro-hydro/diesel hybrid power system in HOMER for the study area. Int J Electra Eng Inf (IJEEI) 3(3), 307 (2011)
2. De Persis, C., Tesi, P.: Formulas for data-driven control: stabilization, optimality, and robustness. IEEE Trans. Autom. Control 65(3), 909–924 (2020)
3. 3. Yousef, A.M., Ebbed, M., Abo-Elymus, F.K., Enzooty, A., Mohamed, M., Abdelwahab, S.A.M.: Optimization of PID controller for hybrid renewable energy system using adaptive sine cosine algorithm. Int. J. Renew. Energy Res. IJRER 10(2), 670– 677 (2020)
4. Wang, H., Hua, L., Guo, Y., Lu, C.: Control of Z-axis MEMS gyroscope using adaptive fractional order dynamic sliding mode approach. IEEE Access 7, 133008–133016 (2019)

5. Gao, P., Zhang, G., Ouyang, H., Mei, L.: An adaptive super twisting nonlinear fractional order PID sliding mode control of permanent magnet synchronous motor speed regulation system based on extended state observer. IEEE Access 8, 53498–53510 (2020)
6. Xu, S.S., Chen, C., Wu, Z.: Study of non-singular fast terminal sliding-mode fault-tolerant control. IEEE Trans. Ind. Electron. 62(6), 3906–3913 (2015)
7. Zhang, X., Zhou, Z.: Integrated fault estimation and fault tolerant attitude control for rigid spacecraft with multiple actuator faults and saturation. IET Control Theory Appl. 13(15), 2365–2375 (2019)
8. Syafaruddin, E., Karatepe, T.H.: Artificial neural network-polar coordinated fuzzy controller based maximum power point tracking control under partially shaded conditions. IET Renew. Power Gener. 3(2), 239–253 (2009)
9. H. Khorasani-Zadeh: Power transformer differential protection scheme based on symmetrical component and artificial neural network. 7th Seminar on neural network applications in electrical engineering, 2004. NEUREL, Belgrade, Serbia, pp. 261–265, (2004)
10. Voloshin, E. A., Voloshin, A. A., Sachdev, S. S., Intensive, A. R., Maksudov B. T., Livshits, S. A.: Increase of efficiency of relay protection reliability in modes with deep saturation of current transformers using the methodology based on the application of Artificial Neural Networks. 2018 International youth scientific and technical conference relay protection and automation (RPA), Moscow, pp. 1–14, (2018)
11. Kalam, R.N., Mubeen, S.M., Al-Durra, A., Hasaean, H.M., Al-Wahedi, K.: Optimisation of controller parameters for grid-tied photovoltaic system at faulty network using artificial neural network-based cuckoo search algorithm. IET Renew. Power Gener. 11(12), 1517–1526 (2017)
12. Yoo, H., Nguyen, T., Kim, H.: Consensus-based distributed coordination control of hybrid AC/DC microgrids. IEEE Trans. Sustain. Energy 11(2), 629–639 (2020)
13. Abdelwahab, S.A.M., Abdellatif, W.S.E., Hamada, A.M.: Comparative analysis of the modified perturb and observe with different MPPT techniques for PV grid connected systems. Int. J. Renew. Energy Res. IJRER 10(1), 156–164 (2020)
14. Ayvaz, E., Kaplan, K., Kundan, M.: An integrated LSTM neural networks approach to sustainable balanced scorecard-based early warning system. IEEE Access 8, 37958–37966 (2020)
15. Chen, J., Park, J.H., Xu, S.: Stability analysis for neural networks with time-varying delay via improved techniques. IEEE Trans. Cybernet. 49(12), 4495–4500 (2019)
16. Yousef, A.M., Ibrahem, H.A., Abo-lours, F.K., Mohamed, M.: Sliding mode control for three phase PV grid connected energy system using LCL filter. Minia J Eng. Technol. (MJET) 36(2), 1 (2017)

17. Zhang, H., Yue, D., Xie, X.: Distributed model predictive control for hybrid energy resource system with large-scale decomposition coordination approach. IEEE Access 4, 9332–9344 (2016)

18. Lobbed, M. M., El-Amary, N. H., Abdelaziz A. Y.: Sliding mode control for hybrid power sources micro-grid. 2019 21st International middle east power systems conference (MEPCON), Cairo, Egypt, pp. 650–655 (2019)

19. Qi, G., Chen, A., Chen, J.: Improved control strategy of inter-linking converters with synchronous generator characteristic in islanded hybrid AC/DC microgrid. CPSS Trans. Power Electron. Appl. 2(2), 149–158 (2017) 20. Awed H., Abdalfatah, S., Hegazy H., Elkholy E. E.: Hybrid PV/ FC system design and simulation. 2019 21st international middle east power systems conference (MEPCON), Cairo, Egypt, pp. 1025–1030 (2019)

21. Mili, L., Hamouda, M., Rahmani, S., Fortin, H., Al-Haddad, B.K.: PWM-based integral sliding-mode controller for unity input power factor operation of indirect matrix converter. J. Power Electron. 17(4), 1048–1057 (2017)

22. Shan, Y., Hu, J., Chan, K.W., Fu, Q., Guerrero, J.M.: Predictive control of bidirectional DC–DC converters and AC/DC interlinking converters—a new control method for PV-wind-battery micro-grids. IEEE Trans. Sustain. Energy 10(4), 1823–1833 (2019)

23. Elba set, A.A., Abdelwahab, S.A.M., Ibrahim, H.A., Eid, M.A.E.: Performance analysis of photovoltaic systems with energy storage systems. Renewable and Green Energy. Springer, Berlin (2019)

24. Pradhan, S., Singh, B., Panigrahi, B.K., Murshid, S.: A composite sliding mode controller for wind power extraction in remotely located solar PV–wind hybrid system. IEEE Trans. Ind. Electron. 66(7), 5321–5331 (2019)

25. Bagchee, H. R., Miralem, M., Hayrapetyan G. B., Talebi, H. A.: Decentralized sliding mode control of WG/PV/FC microgrids under unbalanced and nonlinear load conditions for on- and of-grid modes. IEEE Sits J. 12(4):3108–3119, (2018)

26. Aboody, A.H.K., Elba set, A.A., Abdelwahab, S.A.M.: Effect of dc link capacitance on stand-alone PV system operation with fluctuated dc resistive loads. Port. Said Eng. Res. J. 19(1), 121–128 (2015)

27. Dessouky, S. S., Abdellatif, W. S.E., Abdelwahab S. A. M., Ali M. A.: Maximum power point tracking achieved of DFIG-based wind turbines using perturb and observant method. IEEE international middle-east power systems conference, December 18–20 (2018)

28. Polinder, H., van der Pihl, F.F.A., de Vilder, G., Taner, P.J.: Comparison of direct-drive and geared generator concepts for wind turbines. IEEE Trans. Energy Convers. 21(3), 725–733 (2006)

29. Yousef, A.M., Abo-Elymus, F.K., Enzooty, A., Mohamed, M., Abdelwahab, S.A.M.: Fractional order PI control in hybrid renewable power generation system to three phase grid connection. Int. J. Elect. Eng. Inf. 12(3), 1 (2020)

30. Eid, M. A. E., Elba set, A. A., Ibrahim H. A., Abdelwahab S. A. M.: Modelling, simulation of MPPT using perturb and observe and incremental conductance techniques for stand-alone PV Systems. 2019 21st international middle east power systems conference, Cairo, Egypt, pp. 429–434 (2019)

31. Krohne C., Heaping L.: Phase-locked loop and synchronization. problem-based learning in communication systems using MATLAB and Simulink, IEEE, pp.135–150 (2016)

32. Seidi Khorramabad, S., Bakhshes, A.: Critic-based self-tuning PI structure for active and reactive power control of VSCs in microgrid systems. IEEE Trans. Smart Grid. 6(1), 92–103 (2015)

33. Souza de Santana, E., Jesus Fiats Cerqueira, J., Silva Franklin, T.: Fuzzy and PI controllers in pumping water system using photo voltaic electric generation. IEEE Latin Am. Trans. 12(6), 1049–1054 (2014)

34. Yang, C., Jiang, Y., He, W., Na, J., Li, Z., Xu, B.: Adaptive parameter estimation and control design for robot manipulators with finite-time convergence. IEEE Trans. Ind. Electron. 65(10), 8112–8123 (2018)

35. Leland, R.P.: Adaptive control of a MEMS gyroscope using Lyapunov methods. IEEE Trans. Control Syst. Technol. 14(2), 278–283 (2006)

36. Paiva, G. M. D., Pimentel, S. P., Marra, E. G., Alvarenga, B. P. D., Musette M., Leva, S.: Intra-day forecasting of building-integrated PV systems for power systems operation using ANN ensemble. 2019 IEEE Milan Powertech, Milan, Italy, pp. 1–5, (2019)